Catalysis Science & Technology

Accepted Manuscript

This article can be cited before page numbers have been issued, to do this please use: Y. Hou, H. An, S. Chang and J. Zhang, *Catal. Sci. Technol.*, 2019, DOI: 10.1039/C9CY00094A.




ROYAL SOCIETY OF CHEMISTRY

rsc.li/catalysis

View Article Online
DOI: 10.1039/C9CY00094A

Journal Name

ARTICLE

# Versatile catalysts constructed from hybrid polyoxomolybdates for simultaneously detoxifying sulfur mustard and organophosphate simulants

Received 00th January 20xx,
Accepted 00th January 20xx

DOI: 10.1039/x0xx00000x

www.rsc.org/

**Yujiao Hou, Haiyan An,* Shenzhen Chang, Jie Zhang**

**ABSTRACT**: Chemical warfare agents (CWAs) containing sulfur mustard and organophosphates are among the most toxic materials known to the mankind and have caused lots of casualties during the wars and terrorist attacks. Development of catalysts with selective oxidation and hydrolysis for detoxification of these two types of CWAs is highly desired. Here, we report a series of carboxylic acids modified polyoxomolybdate derivatives with high catalytic performance in the degradation two typical chemical warfare agent simulants: 2-chloroethyl ethyl sulfide (CEES) and diethyl cyanophosphonate (DECP), at room temperature. Our results demonstrate that CEES can high-selectively degrade to the corresponding far less toxic 2-chloroethyl ethyl sulfoxide (CEESO) with the oxidant $H_2O_2$ within 12 minutes, and DECP was almost completely hydrolysed to nontoxic products within 10 minutes. The catalytic activities of these compounds were found to be influenced by the metal cations, carboxylic acid ligands and the heteroatoms of polyoxoanions. The corresponding order is respectively $Co^{2+}$ > $Ni^{2+}$, $Zn^{2+}$, $Mn^{2+}$; PABA > Ala, Ac; AsMo > TeMo.

## 1 Introduction

The destruction of chemical warfare agents (CWAs), including vesicants such as sulfur mustard and nerve agents known as organophosphates, has been always an active area of research owing to their high toxicity and dangerousness to human beings and the environment.[1,2] Sulfur mustard can be effectively destroyed by means of the selective oxidation to the far less toxic sulfoxide.[3,4] Organophosphates can be detoxified by the hydrolysis of the labile P-X bond.[4,5] In view of the hazard in dealing with highly toxic CWAs, effective simulant molecules for CWAs with similar chemical behaviours and architectures are always handled by experiments. Various materials that catalyze selective oxidation of sulfur mustard (or simulants) or hydrolysis of organophosphates (or simulants) into nontoxic corresponding products, have been developed, such as, metal organic frameworks (MOFs), inorganic oxides, zeolites and modified activated carbons.[4-10] Hupp, Farha and coworkers have pioneeringly documented that some Zr-based MOFs (UiO-66, UiO-67, MOF-88 and Nu-1000) can efficiently catalyze the degradation of CWAs, and found the chemical environment around a catalytic active site can obviously influence the catalytic activity.[4,6,7] So far, most reported materials only can catalyze the degradation of one kind of CWAs, either sulfur mustard or nerve agents. Thus, for the practical application concerns, the exploitation of high-efficient broad-spectrum catalysts with multiple detoxification pathways remains a significant challenge.

Polyoxometalates (POMs), as a large group of inorganic metal oxide clusters, bear important applications in catalysis, magnetism, optics, medicine, etc.[11-26] Currently, POMs have been explored as catalytic materials for destroying CWAs by Hill, Nyman, Hu, Liu and other groups, because of their designable structures, versatile redox potentials and tunable acidity/basicity.[27-35] Hill's group firstly reported $H_5PV_2Mo_{10}O_{40}$ can degrade the sulfur mustard gas simulant 2-chloroethyl ethyl sulfide (CEES) in 1994.[27] Since then, some inorganic POMs such as metal-substituted polyoxotungstates ($[(Fe(OH_2)_2)_3(PW_9O_{34})_2]^{9-}$, $[\{PW_{11}O_{39}Zr(\mu\text{-}OH)(H_2O)\}_2]^{8-}$) and polyoxoniobates ($[Nd_6O_{19}]^{8-}$, $K_{12}[Ti_2O_2][GeNb_{12}O_{40}]$) were successively investigated in the catalytic degradation of one kind of CWAs, either by oxidation or by hydrolysis.[28] Recently, a polyoxoniobate–polyoxovanadate complex, $H_{13}[(CH_3)_4N]_{12}[PNb_{12}O_{40}(VO)_2(V_4O_{12})_2]\cdot 22H_2O$, as bifunctional catalyst, was successfully developed to homogeneously degrade sulfur mustard simulants by oxidation and organophosphate simulants *via* hydrolysis.[31] In the search for hererogeneous POM materials for this application, two POM@MOF hybrid materials, $PW_{12}$@NU-1000 and $PV_2Mo_{10}$@MIL-101, were prepared and tested for the degradation of sulfur mustard and its simulant with high conversion but relatively low selectivity.[34,35] Catalytic degradation of CWAs

*College of Chemistry, Dalian University of Technology, Dalian 116023, P. R. China*
Email:anhy@dlut.edu.cn; Fax:+86-411-84657675; Tel:+86-411-84657675
Electronic Supplementary Information (ESI) Synthesis of **13**, **14** and **15**; ORTEP drawing of **1**, **5**, **9**, **10** and **12**, 1D supramolecular chain of **1**, **5**, **9** and **12**; 2D supramolecular sheet of **5** and **12**; IR spectra, UV−Vis diffuse reflective spectra, TG plots, PXRD figures for **1**−**12**; time profile for the oxidative reaction of CEES using **1** under different conditions; kinetic analysis of CEES and DECP; crystal data and structure refinement for **1**−**12**; the formulas of compounds; selected bond lengths and angles for **1**−**12** is provided.

using POM-based compounds has turned into a burgeoning research field in recent years. However, on the one hand, the reported POM-based catalysts still suffered from a lot of problems, such as slow degradation rate, low selectivity and poor recyclability; on the other hand, broad-spectrum POM materials simultaneously catalyzing the degradation of sulfur mustard and nerve agents are still lacking.

One promising method to enhance the catalytic activity and stability of POMs as broad-spectrum catalysts is to graft organic ligands onto POM clusters via covalent bonds to get novel organo-modified materials, which would strengthen the interactions between catalysts and substrates. In 2017, Hill's group prepared a class of hybrid polymers composed of polyoxovanadate clusters covalently bound by 1, 3, 5-benzenetricarboxamide linkers, which catalyze the degradation of CEES and diethyl cyanophosphonate (DECP) within 30 minutes.[36] Very recently, our group found that mixed carboxylic acids modified POMs linked by metal cations can rapidly and high-selectively destroy CEES and DECP, which indicate the great potential of carboxylic acid ligands modified POMs in destroying CWAs.[37] In light of these discoveries, it is of interest to study the new structures and catalytic properties of POMs modified by different carboxylic acid ligands that can provide similar connectivity to the polyoxoanions but different pendent groups. Based on this strategy, we chose carboxylic acid ligands containing pendent amino groups as the organic components, and successfully synthesized a series of new hybrid materials with transition metal cations as linkers: $K_5H[M(H_2O)_m][As^{III}Mo_6O_{21}(PABA)_3]_2{\cdot}nH_2O$ **1**−**4**, $Cs_4X[M(H_2O)_m][Te^{IV}Mo_6O_{21}(PABA)_3]_2{\cdot}nH_2O$ **5**−**8** (M = $Co^{2+}$, $Ni^{2+}$, $Zn^{2+}$, $Mn^{2+}$; X = $Na_2$ **5**, $K_2$ **6**, KH **7**, **8**; PABA = p-aminobenzoic acid), $Rb_2HT[M(H_2O)_6][M(H_2O)_m][As^{III}Mo_6O_{21}(Ala)_2(Ac)]_2{\cdot}nH_2O$ **9**−**11** and $K_2NaH[Mn(H_2O)_3]_2[As^{III}Mo_6O_{21}(Ala)_2(Ac)]_2{\cdot}nH_2O$ **12** (M = $Co^{2+}$, $Ni^{2+}$, $Zn^{2+}$; T = H **9**, **11**, $Na(H_2O)_6$ **10**; Ala = β-Alanine; Ac = Acetic Acid). Compounds **1**−**8** are constituted of PABA ligands modified polyoxomolybdates $[AsMo_6O_{21}(PABA)_3]^{4-}$/$[TeMo_6O_{21}(PABA)_3]^{4-}$ as building units, and $Co^{2+}/Ni^{2+}/Zn^{2+}/Mn^{2+}$ cations as linkers to generate the novel dimeric architectures. Compounds **9**−**12** also have a dimeric structure composed of Ala and Ac ligands modified polyoxomolybdate $[AsMo_6O_{21}(Ala)_2(Ac)]^{4-}$ bridged by metal cations. All these compounds can degrade sulfur mustard simulant CEES with high selectivity within 12 minutes and nerve agent simulant DECP within 10 minutes, representing the rare examples that can simultaneously destroy two kinds of CWAs.

## 2 Experimental section

### Syntheses of $K_5H[M(H_2O)_m][As^{III}Mo_6O_{21}(PABA)_3]_2{\cdot}nH_2O$ (1−4)

In a typical synthesis procedure for **1**−**4**, $Na_2MoO_4$ (0.145 g, 0.6 mmol), $As_2O_3$ (0.0197 g, 0.1 mmol), and PABA (0.0411g, 0.3mmol) were dissolved in 20 mL of water. The pH value of the solution was adjusted from the original pH value of 6.8 to 4.0 with HCl solution under stirring. The solution was stirred for one hour at room temperature. Then, $CoCl_2{\cdot}6H_2O$ (0.0714 g, 0.3 mmol)/$NiCl_2{\cdot}6H_2O$ (0.0678g, 0.3mmol)/$ZnSO_4{\cdot}7H_2O$ (0.0861 g, 0.3 mmol)/ $MnCl_2{\cdot}2H_2O$ (0.0486 g, 0.3 mmol) and KCl (0.022g, 0.3 mmol) were added successively under stirring. Finally, the solution was heated and stirred for one hour at 80 °C. The filtrate was kept undisturbed for two weeks under ambient conditions, and then crystals of **1**−**4** were isolated in about 52% yield (based on Mo). Elemental analyses: calcd for **1** Mo, 33.77; As, 4.39; Co, 1.73; K, 5.73; C, 14.79; N, 2.46; H, 2.39 (%). Found: Mo, 34.03; As, 4.62; Co, 1.66; K, 5.45; C, 14.53; N, 2.27; H, 2.54 (%). FTIR data ($cm^{-1}$): 3360 (s), 1607 (s), 1548 (s), 1413 (w), 1271 (m), 1178(m), 923(m), 894(s), 777 (w), 678 (m), 620(w), 512 (m). Calcd for **2**: Mo, 33.94; As, 4.37; Ni, 1.71; K, 5.70; C, 14.71; N, 2.45; H, 2.44 (%). Found: Mo, 33.76; As, 4.28; Ni, 1.55; K, 5.43; C, 14.48; N, 2.34; H, 2.29 (%). FTIR data ($cm^{-1}$): 3361 (s), 1605 (s), 1546 (s), 1411 (w), 1271 (m), 1178(m), 924(m), 894(s), 776 (w), 678 (m), 619(w), 512 (m). Calcd for **3**: Mo, 33.71; As, 4.39; Zn, 1.91; K, 5.72; C, 14.75; N, 2.46; H, 2.18 (%). Found: Mo, 33.95; As, 4.56; Zn, 1.64; K, 5.94; C, 14.67; N, 2.32; H, 2.07 (%). FTIR data ($cm^{-1}$): 3360 (s), 1606 (s), 1548 (s), 1414 (w), 1272 (m), 1179(m), 922(m), 894(s), 778 (w), 679 (m), 620(w), 513 (m). Calcd for **4**: Mo, 33.46 As, 4.35; Mn, 1.60; K, 5.68; C, 14.64; N, 2.44; H, 2.23 (%). Found: Mo, 35.35; As, 4.22; Mn, 1.69; K, 5.33; C, 14.75; N, 2.18; H, 2.30 (%). FTIR data ($cm^{-1}$): 3358 (s), 1609 (s), 1548 (s), 1411 (w), 1272 (m), 1178(m), 926(m), 895(s), 779 (w), 678 (m), 622(w), 512 (m).

### Syntheses of $Cs_4X[M(H_2O)_m][Te^{IV}Mo_6O_{21}(PABA)_3]_2{\cdot}nH_2O$ (5−8)

In a typical synthesis procedure for **5**−**8**, $Na_2MoO_4$ (0.145 g, 0.6 mmol), $Na_2TeO_3$ (0.022 g, 0.1 mmol), and PABA (0.0411g, 0.3mmol) were dissolved in 20 mL of water. The pH value of the solution was adjusted from the original pH value of 6.5 to 4.0 with HCl solution under stirring. The solution was stirred for one hour at room temperature. Then, $CoCl_2{\cdot}6H_2O$ (0.0714 g, 0.3 mmol)/$NiCl_2{\cdot}6H_2O$ (0.0678g, 0.3mmol)/$ZnSO_4{\cdot}7H_2O$ (0.0861 g, 0.3 mmol)/$MnCl_2{\cdot}2H_2O$ (0.0486 g, 0.3 mmol) and CsCl (0.034g, 0.2mmol) and KCl (0.007g, 0.1mmol) were added successively under stirring. Finally, the solution was heated and stirred for one hour at 80 °C. The filtrate was kept undisturbed for two weeks under ambient conditions, and then crystals of **5**−**8** were isolated in about 45% yield (based on Mo). Elemental analyses: calcd for **5**: Mo, 29.03; Te, 6.43; Co, 1.49; Cs, 13.40; Na, 1.16; C, 12.72; N, 2.12; H, 2.19 (%). Found: Mo, 29.43; Te, 6.62; Co, 1.66; Cs, 13.15; Na, 1.29; C, 12.33; N, 2.27; H, 2.34 (%). FTIR data ($cm^{-1}$): 3385 (s), 1604 (s), 1533 (s), 1406 (s), 1281 (w), 1178(m), 903(s), 768 (w), 728 (w), 637(s), 513 (w). Calcd for **6**: Mo, 28.88; Te, 6.62; Ni, 1.52; Cs, 13.79; K, 2.03; C, 13.09; N, 2.18; H, 1.83 (%). Found: Mo, 28.53; Te, 6.49; Ni, 1.77; Cs, 13.51; K, 2.12; C, 12.83; N, 2.07; H, 1.92 (%). FTIR data ($cm^{-1}$): 3384 (s), 1604 (s), 1535 (s), 1406 (s), 1282 (w), 1178(m), 905(s), 768 (w), 728 (w), 637(s), 516(w). Calcd for **7**: Mo, 29.84; Te, 6.61; Zn, 1.69; Cs, 13.78; K, 1.01; C, 13.07; N, 1.45; H, 1.96 (%). Found: Mo, 29.44; Te, 6.44; Zn, 1.77; Cs, 13.31; K, 1.21; C, 13.33; N, 1.32; H, 2.24 (%). FTIR data ($cm^{-1}$): 3382 (s), 1606 (s), 1533 (s), 1406 (s), 1286 (w), 1178(m), 905(s), 768 (w), 728 (w), 635(s), 513 (w). Calcd for **8**: Mo, 29.37; Te, 6.51; Mn, 1.40; Cs, 13.56; K, 1.00; C, 12.87; N, 2.14; H, 2.13 (%). Found: Mo, 29.46; Te, 6.29; Mn, 1.58; Cs, 13.42; K, 1.21; C, 12.54; N, 2.31; H, 2.23 (%). FTIR data ($cm^{-1}$):

View Article Online
DOI: 10.1039/C9CY00094A



3387 (s), 1601 (s), 1536 (s), 1406 (s), 1283 (w), 1178(m), 907(s), 768 (w), 728 (w), 638(s), 513 (w).

**Syntheses of $Rb_2HT[M(H_2O)_6][M(H_2O)_m][As^{III}Mo_6O_{21}(Ala)_2(Ac)]_2{\cdot}nH_2O$ (9−11)**

In a typical synthesis procedure for **9**−**11**, $Na_2MoO_4$ (0.145 g, 0.6 mmol), $As_2O_3$ (0.0197 g, 0.1 mmol), Ala (0.0267g, 0.3mmol) were dissolved in 20 mL of water. The pH value of the solution was adjusted from the original pH value of 6.8 to 4.0 with 4 M HCl solution under stirring. The solution was stirred for one hour at room temperature. Then, $Co(OAc)_2{\cdot}4H_2O$ (0.0747 g, 0.3 mmol)/$Ni(OAc)_2{\cdot}4H_2O$(0.0747g, 0.3mmol)/$Zn(OAc)_2{\cdot}2H_2O$ (0.0659 g, 0.3 mmol), and RbCl (0.024g, 0.2mmol) were added successively under stirring. Finally, the solution was heated and stirred for one hour at 80 °C. The filtrate was kept undisturbed for two weeks under ambient conditions, and then crystals of **9**−**11** were isolated in about 39% yield (based on Mo). Elemental analyses: calcd for **9**: Mo, 36.95; As, 4.81; Co, 3.78; Rb, 5.48; C, 6.16; N, 1.80; H, 2.52 (%). Found: Mo, 36.51; As, 4.67; Co, 3.47; Rb, 5.13; C, 5.99; N, 1.95; H, 2.87 (%). FTIR data ($cm^{-1}$): 3439 (s), 3150 (m), 1595 (s), 1432 (s), 1401 (w), 1276 (m), 1240(m), 1173(m), 929(m), 889(s), 762 (w), 674 (m), 627(w), 505 (m). Calcd for **10**: Mo, 34.51; As, 4.49; Ni, 3.52; Na, 0.69; Rb, 5.12; C, 5.76; N, 1.68; H, 2.99 (%). Found: Mo, 34.82; As, 4.55; Ni, 3.82; Na, 0.62; Rb, 5.32; C, 6.10; N, 1.78; H, 2.72 (%). FTIR data ($cm^{-1}$): 3441 (s), 3151 (m), 1596 (s), 1434 (s), 1402 (w), 1275 (m), 1241(m), 1172(m), 929(m), 889(s), 763 (w), 675 (m), 628(w), 504 (m). Calcd for **11**: Mo, 36.37; As, 4.73; Zn, 4.13; Rb, 5.40; C, 6.07; N, 1.77; H, 2.61 (%). Found: Mo, 36.21; As, 4.52; Zn, 4.40; Rb, 5.69; C, 6.28; N, 1.70; H, 2.76 (%). FTIR data ($cm^{-1}$): 3439 (s), 3149 (m), 1592 (s), 1433 (s), 1402 (w), 1277 (m), 1241(m), 1173(m), 929(m), 889(s), 764 (w), 675 (m), 627(w), 506 (m).

**Syntheses of $K_2NaH[Mn(H_2O)_3]_2[As^{III}Mo_6O_{21}(Ala)_2(Ac)]_2{\cdot}12H_2O$ (12)**

The synthetic procedure for **12** was similar to that used for **9**, with $Mn(OAc)_2{\cdot}2H_2O$(0.0804g, 0.3 mmol) instead of $Co(OAc)_2{\cdot}4H_2O$ (0.0747g, 0.3 mmol) and RbCl was replaced by KCl (0.016g 0.2mmol). The filtrate was kept undisturbed for two weeks under ambient conditions, and then light yellow crystals of **12** were isolated in about 38% yield (based on Mo). Calcd for **12**: Mo, 38.59; As, 5.02; Mn, 3.68; K, 2.62; Na, 0.77; C, 6.44; N, 1.88; H, 2.40 (%). Found: Mo, 38.75; As, 4.84; Mn, 3.42; K, 2.48; Na, 0.73; C, 6.33; N, 1.75; H, 2.66 (%). FTIR data ($cm^{-1}$): 3442 (s), 3147 (m), 1592 (s), 1431 (s), 1402 (w), 1276 (m), 1241(m), 1173(m), 929(m), 891(s), 762 (w), 672 (m), 627(w), 505 (m).

**General methods for catalyzing degradation of CEES and DECP**

CEES oxidation: POM catalyst (2.5 μmol), $H_2O_2$ (0.3 mmol), CEES (0.25 mmol), and acetonitrile (0.5 mL) were put in a glass bottle. The catalytic reaction was carried out at room temperature for 12 minutes. Hydrolysis DECP: POM catalyst (0.6 μmol), DECP (1 mmol), DMF (0.6 mL) and $H_2O$ (50 μL) were put in a glass bottle. The catalytic reaction was carried out at room temperature for 10 minutes. After the catalytic reaction was finished, GC-FID, GC-MS and $^1$HNMR were used to analyze the resulting mixture.

## 3 Results and discussion

**Synthesis**

In this paper, we got twelve hybrid compounds based on PABA ligands modified POMs $[AsMo_6O_{21}(PABA)_3]^{4-}$/$[TeMo_6O_{21}(PABA)_3]^{4-}$, and Ala and Ac ligands modified POMs $[AsMo_6O_{21}(Ala)_2(Ac)]^{4-}$. In **1**−**12**, these carboxylic acids modified POMs were joint together to form interesting dimeric structures through the linkage of transition metal cations ($Co^{2+}$, $Ni^{2+}$, $Zn^{2+}$, $Mn^{2+}$). Other metal cations were also attempted to be introduced to this reaction system. For example, when $Cu^{2+}$ cation was used, only coordination complex containing $Cu^{2+}$ and organic ligands was produced. Rare earth metal cations, such as $La^{3+}$, $Ce^{3+}$, and $Nd^{3+}$, were also attempted to be the linkages to synthesize the similar compounds, however only precipitation was obtained. If no transition metal cations were added to the reaction solutions of **1**−**4**, the poor-quality crystal compound $K_3[AsMo_6O_{21}(PABA)_3]{\cdot}nH_2O$ (compound **13**) with $K^+$ as cations was synthesized. Above parallel experiments demonstrate that metal cations play an important role for the formation of these hybrid compounds. In the synthetic process of **9**−**12**, Ala and Ac ligands were simultaneously added to the reaction solution. If Ac ligand was not added, hybrid compounds based on only Ala modified POM $K_6Na_2H_2[(H_2O)_6Co][AsMo_6O_{21}(Ala)_3]_4{\cdot}41H_2O$ (**14**) were isolated, which show a mono-supporting structure. Thus, the metal cations $Co^{2+}$/$Ni^{2+}$/$Zn^{2+}$/$Mn^{2+}$ and the organic ligands play crucial roles in constructing the dimers with carboxylic acid ligands modified POM subunits.

The alkali metal counter cations also are important to the preparation of these compounds. In the synthesis of **1**−**4**, the $K^+$ cations need to be introduced to the reaction system because the $K^+$ cation participates in the formation of **1**−**4**. In the absence of $K^+$, no crystal could be formed. During the preparation of **5**−**8**, the $Cs^+$ and $K^+$ cations were all necessary to get the similar dimeric structures with **1**−**4**. If no $Cs^+$ cation was added to the reaction solution, only precipitate was obtained, and only compound **5** can be obtained without $K^+$ in the existence of $Cs^+$. When $Cs^+$ cation was added to the reaction system of **1**−**4** in the existence of $K^+$ cations, no influences on the final architectures were found. Besides, in the synthesis of **9**−**11**, the $Rb^+$ cation was the indispensable component, whereas the $K^+$ was the necessary element in the preparation of **12**. If no $Rb^+$ was introduced to the reaction system of **9**−**11**, the poor-quality crystals would be obtained.

In addition, the parallel experiments were proceeded and indicated that the reaction stoichiometry, temperature and pH value can also influence the quality of the crystals. In the synthetic process, compounds **1**−**12** can be well obtained in one pot reaction of $Na_2MoO_4$, $As_2O_3$/$Na_2TeO_3$, PABA (Ala and Ac) and TM with the ratio of Mo/As(Te)/PABA/TM = 6:1:3:3. The quality of crystals and the yields will vary considerably over the ratio of these raw materials. The optimal reaction temperature is 80 °C. At higher temperature (100 °C), compounds were synthesized with poor quality crystals, at room temperature (25 °C), no reaction

occurred. The optimal pH value is from 3.4 to 4.5, whether for a low pH (pH = 2.5) or high pH (pH = 5.5), only precipitations can be obtained.

**Crystal structures of 1−12**

Single crystal X-ray analyses reveal that compounds **1**−**8** crystallize in the space group *P*-1. The eight compounds include the similar polyoxoanion unit $\{ZMo_6O_{21}\}$ (Z = As, Te), which are composed of a ring of six almost coplanar edge-sharing and corner-sharing $MoO_6$ octahedra. In this unit, the central As/Te atom is situated slightly above the $MoO_6$ unit and connects to three oxygen atoms to generate a trigonal-pyramidal molecular geometry. This coordinated mode and coordination geometry of $\{ZMo_6O_{21}\}$ are obviously different from the classic Anderson-type POMs. Next, the polyoxoanions $\{ZMo_6O_{21}\}$ are covalently coordinated to three carboxylic acid ligands (PABA) via the carboxyl units to form the single-side organically modified POMs $\{ZMo_6O_{21}(PABA)_3\}$ in **1**−**8** (Fig. 1a). Given compounds **1**−**8** have similar structures, only compounds **1** and **5** were taken as examples to be discussed here. In the PABA modified POMs, the average bond length of Mo-Ob (2.308Å) (μ2-O of Mo) in **1** and Mo-Ob (2.273Å) (μ2-O of Mo) in **5** are akin to other carboxylates modified POM derivatives, and distinctly longer than the initial Mo-Ot (1.703 Å) (terminal oxygen of Mo). In addition, three classes of O atoms exist in the cluster in view of the different coordinated manners and environment. Hence, the Mo-O bond lengths are divided into three different groups: Mo–Ot 1.704(4)–1.731(5) Å, Mo–Ob 1.905(5)–2.337(6) Å, Mo–Oc 2.164(3)–2.232(4) Å in **1**; Mo–Ot 1.709(5)–1.724(6) Å, Mo–Ob 1.911(4)–2.286(4) Å, Mo–Oc 2.226(3)–2.277(4) Å in **5**. The angles of O-As-O change from 95.78(18) to 96.67(18) in **1**; the angles of O-Te-O change from 93.70(18) to 94.04(18) in **5**. Corresponding to the reported study, the bond lengths and angles of this report are within the reasonable ranges.

In the asymmetric unit of **1**, it contains one crystallographically independent $[AsMo_6O_{21}(PABA)_3]^{3-}$ polyoxoanion, half one $Co^{2+}$ cation, and two and half $K^+$ cations (Fig. S1). The asymmetric unit of **5** was similar with **1**, except $Cs^+$ and $Na^+$ were cations instead of the $K^+$ (Fig. S2). Unique Co(1) ion in **1** (**5**) is coordinated to three water molecular [Co–OW 1.997(6)–2.107(4) Å in **1**; 2.056(5)–2.165(5) Å in **5**] and two terminal oxygen atoms originated from two polyoxoanions [Co–O 2.000(6)–2.046(5) Å in **1**; 2.110(5)–2.133(5) Å in **5**] to generate a distorted square pyramidal geometry. Then, two PABA modified POMs were linked together to produce a dimer by Co–O–Mo bonds, related by an inversion center (Fig. 1b). Such dimers based on carboxylic acids modified POMs and metal cations have never been known up to now. Interestingly, strong hydrogen bonds exist between the N atoms of PABA and O atoms of polyoxoanions (N3−H···O26 = 2.920 Å in **1**; N1−H···O12 = 2.886 Å in **5**), generating a 1D supramolecular chain (Fig. S3, S4). These 1D chains are joint together to produce a 2D layer (Fig. 1c, S5) also through the hydrogen bonds between the N atoms of PABA and O atoms of polyoxoanions (N2−H···O7 = 2.879 Å, O1W−H···O10 = 2.940 Å in **1**; N1−H···O9 = 2.737 Å in **5**).

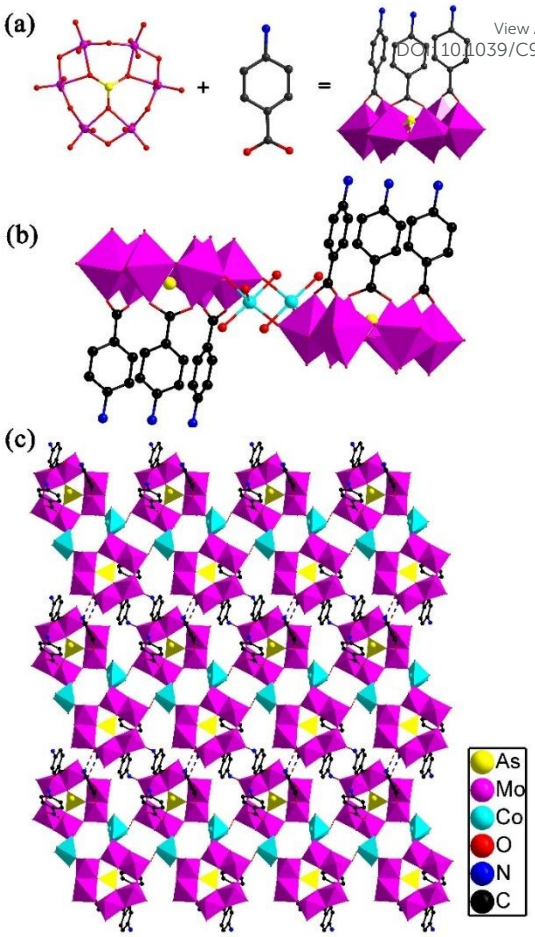


**Fig. 1** a) The direct self-assembly protocol for the synthesis of carboxylic acid ligands modified POM $[AsMo_6O_{21}(PABA)_3]^{4-}$; b) Ball-stick and polyhedral representation of dimeric polyanion for **1**; c) View of the 2D supramolecular framework showing the hydrogen bonds. (color code: As yellow, Mo purple, Co light blue, O red, N blue, C black).

When Ala and Ac ligands were used as the organic components, compounds **9**−**12** were isolated, which crystallize in the space group *P*21/c and have the same polyoxoanion unit $\{AsMo_6O_{21}\}$ with compounds **1**−**4**. Then two different carboxylate ligands (two protonate Ala and one Ac) were coordinated together with the polyoxoanion $\{AsMo_6O_{21}\}$ on the one side to form the mix carboxylic acids modified POMs $[AsMo_6O_{21}(Ala)_2(Ac)]^{4-}$ (Fig. 2a). Similar to compounds **1**−**4**, the Mo-O bond lengths are classified into three kinds: Mo–Ot 1.700(3)–1.725(6) Å, Mo–Ob 1.893(3)–2.328(6) Å and Mo–Oc 2.184(6)–2.225(4) Å in **9**. The angles of O-As-O change from 96.1(3) to 96.6(3) in **9**. The asymmetric unit in **9**−**11** contain one crystallographically independent $[AsMo_6O_{21}(Ala)_2(Ac)]^{4-}$ polyoxoanion, one $Co^{2+}$/$Ni^{2+}$/$Zn^{2+}$ cation and one $Rb^+$ (compound **10** also has half one $Na^+$) (Fig. S6). The asymmetric unit of **12** was similar with **9** except the $Rb^+$ was replaced by $K^+$ (Fig. S9). A dimeric structure was formed through two modified POMs jointed together by M–O–Mo bonds in **9**−**12** (Fig. 2b). However, $Co^{2+}$ cations in **9** and **1** (**5**) displayed different coordination behaviors, thus producing different dimeric structures. The unique $Co^{2+}$ cation in **9** is defined by three O atoms originated from the polyoxoanions [Co–O 2.103(5)–2.201(6) Å]

and three water molecules [Co–OW 2.193(5)–2.277(5) Å] to form the distorted octahedron, which is different from the coordination mode for **1** (three water molecules and two terminal oxygen atoms to produce the distorted square pyramidal). Strong hydrogen bonds between N atoms of Ala and O atoms of polyoxoanions produce a 1D supramolecular chain in **9** (Fig. S8) (N2−H···O6 = 2.778 Å). These 1D chains were further linked together to form a 2D layer (Fig. 2c) through the hydrogen bonds (O2W−H···O18 = 2.854 Å).

Bond valence sum (BVS) calculations indicate that the oxidation states of Mo, As and Te are respectively +6, +3, +4, and Co/Ni/Zn/Mn are +2.

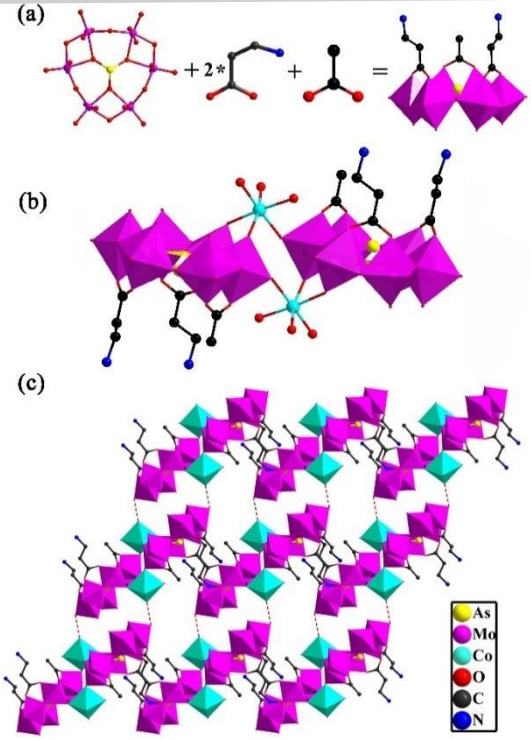


**Fig. 2** a) The direct self-assembly protocol for the synthesis of carboxylic acid ligands modified POM $[AsMo_6O_{21}(Ala)_2(Ac)]^{4-}$; b) Ball-stick and polyhedral representation of dimeric polyanion for **9**; c) View of the 2D supramolecular framework showing the hydrogen bonds. (color code: As yellow, Mo purple, Co light blue, O red, N blue, C black).

## TGA and PXRD Characterization

The TGA of these compounds are shown in Fig. S18~S20, which demonstrate these compounds display multistep weight loss processes. The total weight loss of 34.9%, 35.2%, 35.0%, 34.7%, 30.1%, 35.1%, 35.4%, 37.4%, 27.9%, 31.0%, 28.3%, and 26.8% meet the calculated weight loss 34.4%, 34.8%, 34.4%, 35.2%, 30.7%, 34.8, 35.9%, 37.2%, 27.4%, 31.3%, 28.1%, and 26.5% from 50 to 800 °C. Take compound **1** as an example, the first weight loss from 50 to 150 °C is 9.5%, corresponding to all the lattice water and partial coordinated water. The second weight loss of 7.5% from 150 °C to 380 °C was mainly attributed to the remaining coordinated water and partial organic ligands. The last weight loss of 21.5% from 380 °C to 750 °C arose from the loss of organic ligands and partial oxygen molecules.

Fig. S21~S23 displayed the PXRD patterns of compounds **1**–**12**. The calculated and experimental patterns of the diffraction peaks matched well, which certified the phase purities of these compounds. In addition, the similar diffraction peaks among **1**–**8** indicate the isostructural nature of these compounds, which are different with those of **9**–**12**. Moreover, these conclusions agree with the results obtained from the single crystal X-ray analysis.

## Catalytic oxidation study

Given CEES is regarded as an effective simulant molecule for sulfur mustard, we attempted to investigate the catalytic oxidation degradation effect of these compounds for CEES. To perform the oxidative degradation reaction, CEES (0.25 mmol), catalyst (2.5 μmol), $H_2O_2$ (oxidant 0.3 mmol), and naphthalene (internal standard 0.25 mmol) were dispersed in acetonitrile (0.5 ml) at room temperature, the reaction was detected by gas chromatography (GC). We were delighted to find out that CEES can almost entirely be rapidly degraded to the far less toxic product 2-chloroethyl ethyl sulfoxide (CEESO) and hardly any 2-chloroethyl ethyl sulfone ($CEESO_2$) within 12 minutes. Fig. 3b, 3c, 3d illustrate the conversion of the oxidation of CEES with compounds **1**−**12** and blank, which indicate that these compounds can efficiently degrade the CWAs simulant molecule CEES within 12 minutes. Compound **1** shows the best catalytic activity, and can oxidize 98.9% of CEES into the far less toxic product CEESO (sele.% = 98.0%); compounds **5** has better catalytic activity than other isostructural species **6**–**8**, making 97.4% of CEES degrade to CEESO (sele.% = 96.5%); compound **9** also displays better activity than **10**–**12**, making 93.8% of CEES degrade to CEESO (sele.% = 89.0%) at 12 minutes. There appeared to be negligible activity without catalyst. GC-FID signals were recorded in Fig. 4a, showing the process of the oxidative degradation for CEES in the presence of **1**, which indicated CEES is almost entirely converted to the corresponding products within 12 minutes under mild conditions. In addition, Fig. 4b also displays the progress of the degradation reaction of CEES in the presence of **1** by $^1H$ NMR spectroscopy. And it can be employed to monitor the reaction process, confirm the products and further ascertain the accuracy of the reaction. The reaction processes at 6 and 12 minutes were performed in $CDCl_3$ in the $^1H$ NMR spectrum. To further illuminate the reaction, the $^1H$ NMR spectra of the pure CEES, CEESO and $CEESO_2$ were also detected. The spectrum contrast of actual reaction and pure compounds further demonstrates that CEES can be almost oxidized to the far less toxic CEESO within 12 minutes. Subsequently, to explore the active components of compound **1** in the selective oxidation degradation of CEES, we investigated the catalytic effect of PABA, compound **13** ($K_3[AsMo_6O_{21}(PABA)_3]\cdot nH_2O$), and $CoCl_2$ salt. The formula of **13** was deductive by IR spectrum and EDS data because of the poor crystal quality (Fig. S14). As shown in Fig. 5, the ligand PABA alone oxidizes very little CEES, and compound **13** can convert 72.0% CEES with 82.0% selectivity, which are all lower than that for **1**. Furthermore, the transition metal salt $CoCl_2$ also oxidized only 13.0% CEES with the selectivity 74.0%. Above all, we can speculate that the combination of Co site and PABA modified POM can promote the catalytic oxidation reaction with rapid reaction process and wonderful selectivity in the degradation

of CEES.

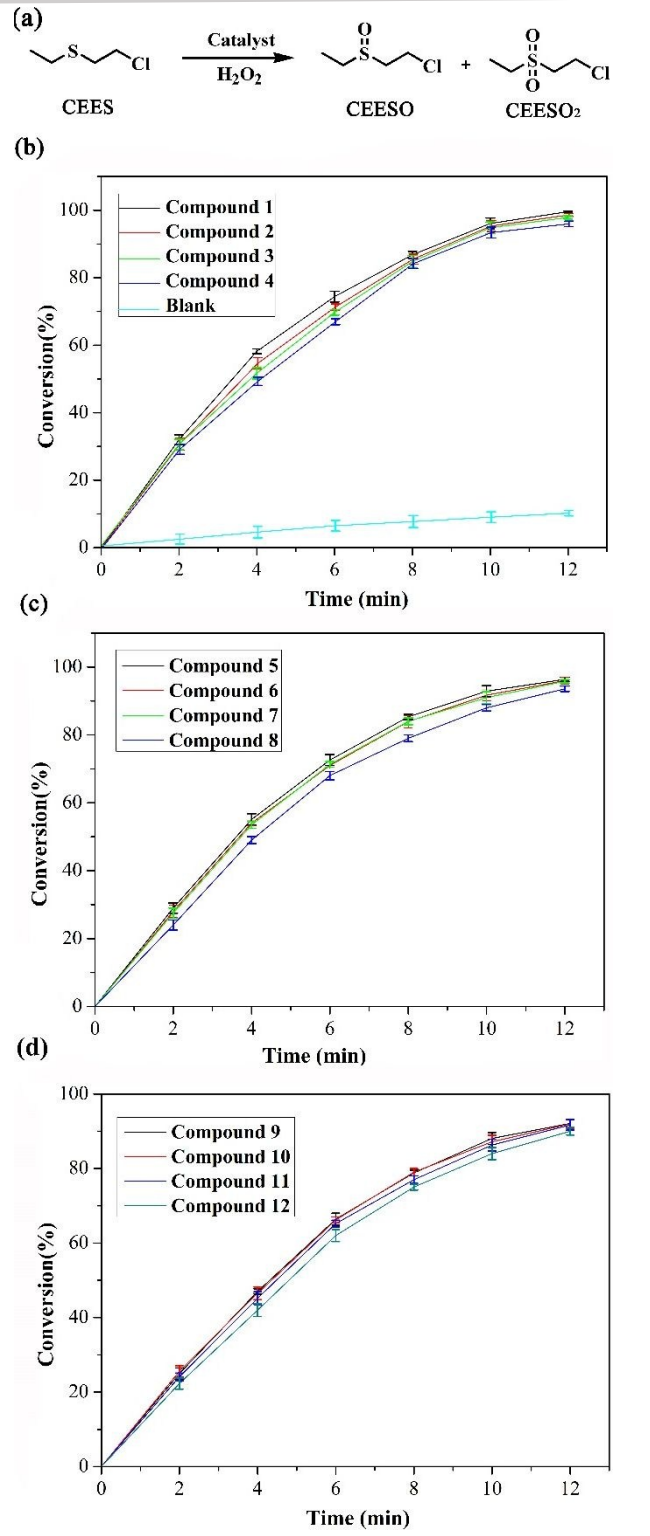


**Fig. 3** a) Catalytic oxidation pathway of CEES to CEESO and $CEESO_2$; b, c, d) The conversion of CEES oxidation for compounds **1**–**12** and blank. Reaction conditions: 0.25 mmol CEES, 2.5 μmol catalyst, 0.25 mmol naphthalene (internal standard), 0.3 mmol $H_2O_2$ and 500μL $CH_3CN$ at room temperature for 12 min.

Furthermore, the catalytic oxidation activity of **1** was compared with that of **5** constructed from $\{TeMo_6(PABA)_3\}$ and $Co^{2+}$, and that of **9** based on $\{AsMo_6(Ala)_2(Ac)\}$ and $Co^{2+}$ for the degradation of CEES (Table 1). The catalytic activity (conv.% = 98.9%, sele.% = 98.0%) of compound **1** is higher than the activity (97.4%, 96.5%) of compound **5**, indicates that the central hetero atom produces certain role on the CEES oxidation. In contrast, the catalytic activity of compound **1** is obviously higher than the activity (93.8%, 89.0%) of compound **9**, which might be due to the carboxylic acid ligands with different structures. PABA is the coordinated carboxylic acid in **1**, and Ala and Ac are the organic ligands in **9**, which reveals that PABA ligand modified POM is more in favour of the catalytic reaction.

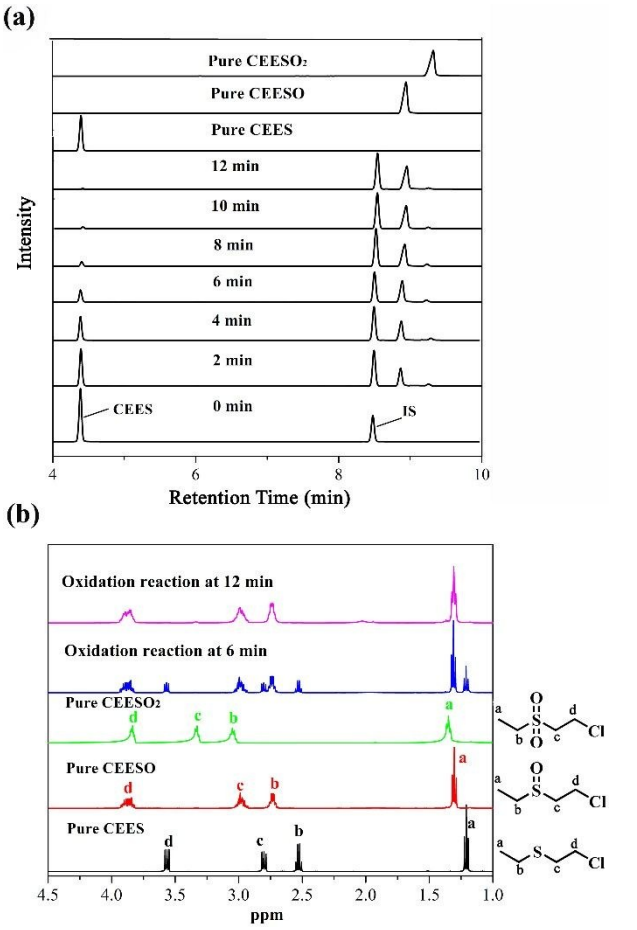


**Fig. 4** a) GC-FID signals indicating the progress of the oxidation of CEES (4.56 min) to CEESO (8.920 min) and $CEESO_2$ (9.23), and internal standard (8.495 min, naphthalene) in the presence of **1**; b) Selected regions of the $^1H$ NMR spectra of CEES, CEESO, $CEESO_2$ oxidation reaction (without internal standard) at 6 min and oxidation reaction (without internal standard) at 12 min with two compounds in $CDCl_3$. The peaks used for calculation are labeled with chemical shift.

For understanding how the carboxylic acid ligands impact the catalytic activity, two compounds, $K_6Na_2H_2[(H_2O)_6Co][AsMo_6O_{21}(Ala)_3]_4{\cdot}41H_2O$ (**14**) with alanine ligand (Ala) and $K_{10}[(H_2O)_6Co][AsMo_6O_{21}(PHBA)_3]_2{\cdot}23H_2O$ (**15**) with p-hydroxybenzonic acid (PHBA) were prepared and detected for the catalytic oxidation degradation of CEES. Compounds 14 and 15 can respectively degrade 73.0% and 92.1% of CEES with 94.2% and 93.4% selectivity under similar conditions (Fig. 5). The catalytic activities of compounds **14** and 15 are observably lower than that of

compound **1**. The three compounds contain the same $\{AsMo_6O_{21}\}$ anion, the $Co^{2+}$ cation, but different carboxylic acid ligands. By comparing the structure of PABA ligand in 1 with PHBA ligand in 15, amino group ($NH_2$) is more advantageous than hydroxyl group (OH) for the catalytic oxidation of CEES; in the contrast of PABA in 1 and Ala in 14, the carboxylic acid ligand with aromatic group is more beneficial. From the catalytic results, it can be found that PABA ligand with aromatic amine is better than Ala, PHBA and Ac ligands for the oxidation of CEES, when these ligands are used to modify POMs. These results manifested carboxylic acid ligands that modified POMs play a key role in the oxidation of CEES.

**Table 1. Comparison of CEES decomposition by different materials.**

| Catalyst | Conversion (%) | Sulfoxide selectivity (%) |
|---|---|---|
| Compound **1** | 98.9 | 98.0 |
| Compound **5** | 97.4 | 96.5 |
| Compound **9** | 93.8 | 89.0 |
| Compound **13** | 72.0 | 82.0 |
| Compound **14** | 92.1 | 93.4 |
| Compound **15** | 73.0 | 94.2 |

Reaction conditions: CEES (0.25 mmol, 1 equiv), catalyst (1 mol%), $H_2O_2$ (1.2 equiv), naphthalene (0.25 mmol) and acetonitrile (0.5 mL), for 12 min, at room temperature.

Then, other elements that influence the activity of these compounds were also investigated. When we compared compound **9** with compound **14**, which constructed from the same polyoxoanion $\{AsMo_6O_{21}\}$ and organic ligand Ala, we found that compound **9** with more $Co^{2+}$ cation displayed higher catalytic activity. This result exhibits $Co^{2+}$ cation is the catalytic active site, and the higher quantity has the higher activity. However, when focusing on the catalytic effect of compounds **1** and **9**, the catalyst **9** with more $Co^{2+}$ shows lower conversion and selectivity of CEES, which might be attributed to the differences of carboxylic acid ligands playing the leading part. So, the cooperation between $Co^{2+}$ and PABA modified $\{AsMo_6O_{21}\}$ in **1** promotes the catalytic performance in the catalytic degradation process for CEES.

In light of the abovementioned consequences and the previous researches, especially investigated widely based on POMs, the peroxo-metal species play an important role in the catalytic oxidation reaction in the presence of POMs and $H_2O_2$.[31,32,38] To understand the reaction mechanism, radical scavengers, such as 2,6-Di-tert-butyl-p-cresol, diphenylamine and p-benzoquinone were introduced to the catalytic systems, respectively. The conversion of CEES remained unchanged after adding the scavengers, indicating that no radical species are responsible for the oxidation reaction of CEES. In this regard, we summarized a possible nonradical reaction mechanism of CEES oxidation degradation in Fig. 6a. Indeed, the interaction between **1** and $H_2O_2$ was confirmed by the changes of the UV-vis spectrum of the mixture solution of before and after $H_2O_2$ was added to the solution of **1** (248 → 253nm, 546 → 552nm) (Fig. 6b, c). Therefore, the catalyst interacts with $H_2O_2$ to form an active peroxomolybdenum and peroxocobalt species, which lead to the reaction with S atom of CEES, generating the corresponding products.

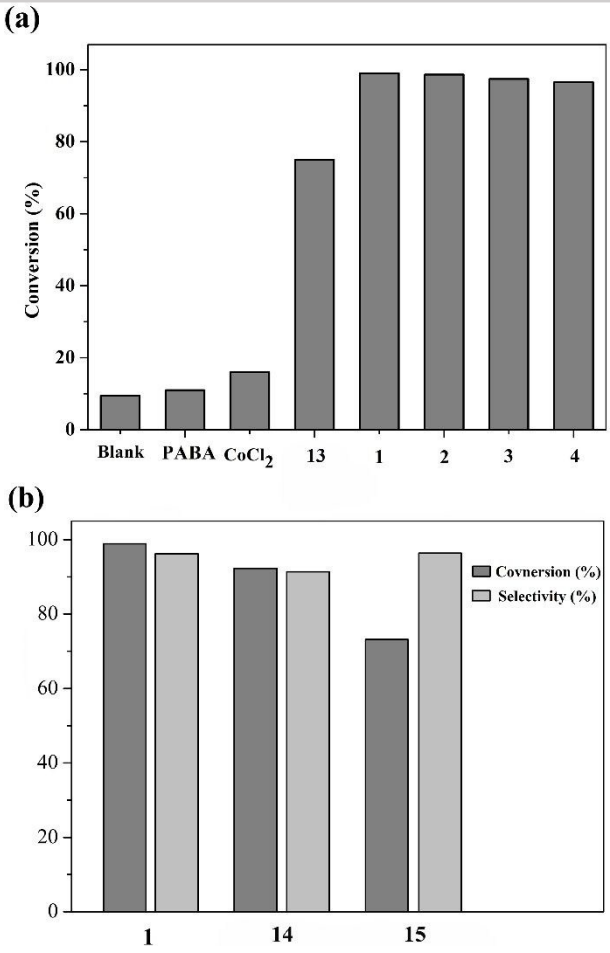


**Fig. 5** a) The oxidation of CEES by different catalysts; b) The conversion and selectivity of CEES oxidation for different catalysts. Reaction conditions: 0.25 mmol CEES, 2.5 μmol catalyst, 0.25 mmol naphthalene (internal standard), 0.3 mmol $H_2O_2$ and 500 μL $CH_3CN$ at room temperature for 12 min.

Then, we continued to study the factors that influence the degradation reaction with compound **1** as catalyst. Obviously, both the quantity of catalyst and $H_2O_2$ restrict the catalytic reaction. The optimized catalyst loading for compound **1** is 1% equiv (Fig S26). The conversion of CEES was lowered to 73.0% when the catalyst loading was decreased from 1% to 0.8% equiv in 12 min. The conversion of CEES was almost unchanged when the catalyst loading was increased from 1% to 1.2% equiv. This phenomenon is often observed in the heterogeneous catalytic system.[31,32,39] And the feasible ratio of oxidant to CEES is 1.2 to 1.1. When the oxidant was lowered to 0.8% equiv, the conversion of CEES was observed to be 70.5 % and keep almost constant with high selectivity (Fig. S27). When the oxidant $H_2O_2$ was replaced to TBHP, the conversion we found were far below than that for $H_2O_2$. The catalytic oxidation reaction kinetics of CEES was next investigated. Fig. 3 displays the time profiles for the oxidation reaction process of CEES. $Ln(C_t/C_0)$ against the reaction time shows a linear correlation, which indicates that the oxidation of

CEES accords with a first-order reaction ($C_t$ and $C_0$ represent the CEES concentration at some time and at the begin time). The first-order kinetics constants $k_1$~$k_{12}$ for **1**−**12** are 0.38211 $min^{-1}$, 0.3479 $min^{-1}$, 0.30719 $min^{-1}$, 0.2804 $min^{-1}$, 0.33069 $min^{-1}$, 0.27797 $min^{-1}$, 0.31077 $min^{-1}$, 0.22987 $min^{-1}$, 0.21809 $min^{-1}$, 0.21486 $min^{-1}$, 0.20998 $min^{-1}$, and 0.19482 $min^{-1}$, respectively (Fig. S28~S30).

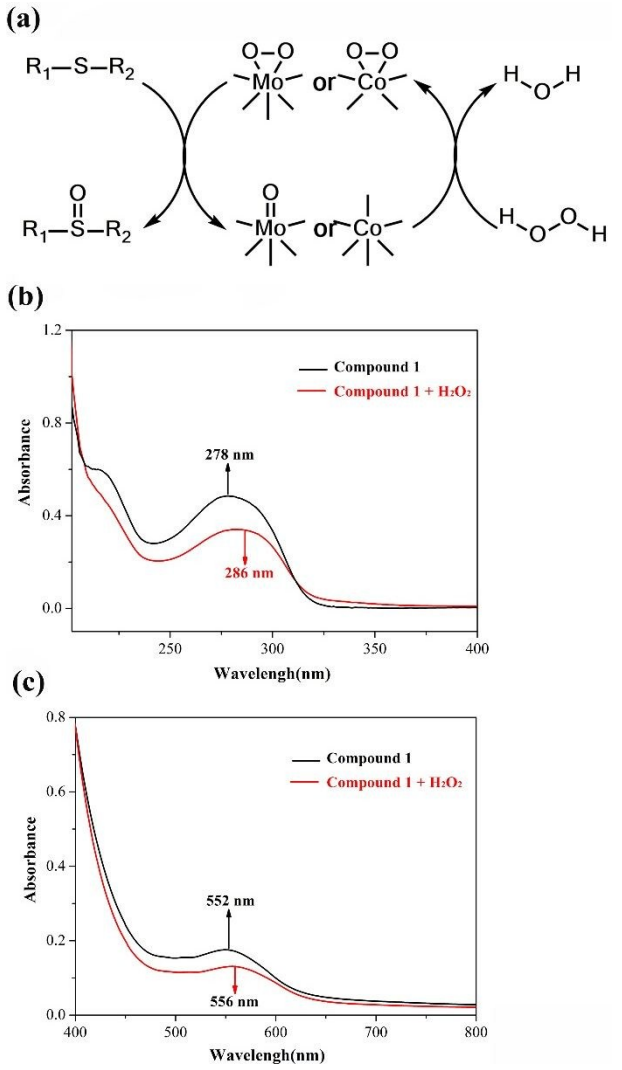


**Fig. 6** a) Proposed mechanism of the catalytic oxidation of CEES; b) UV-vis spectra of compound **1** in dimethyl sulfoxide with one-drop portions of $H_2O_2$ on the UV region (200−400 nm); c) UV-vis spectra of compound **1** in dimethyl sulfoxide with one-drop portions of $H_2O_2$ on the vision region (400−800 nm). The red shift of the absorption spectrum after adding $H_2O_2$ show the interactions between compound **1** and $H_2O_2$.

The recyclability and stability of the heterogeneous catalysts were further researched in the catalytic process. The catalyst was easily collected by simple filtration. In the following 10 cycles, the conversion and selectivity of CEES keep almost constant using the recovered catalyst, which demonstrate wonderful cycling stability of **1** (Fig. 7a). And the filtrate showed no catalytic activity on the oxidation of CEES in the similar situation. Moreover, the IR spectra and the PXRD patterns of **1** keep virtually identical before and after the catalytic process (Fig. 7b, c). Thus, the abovementioned results manifest that compound **1** is an excellent heterogeneous oxidation catalyst of CEES.

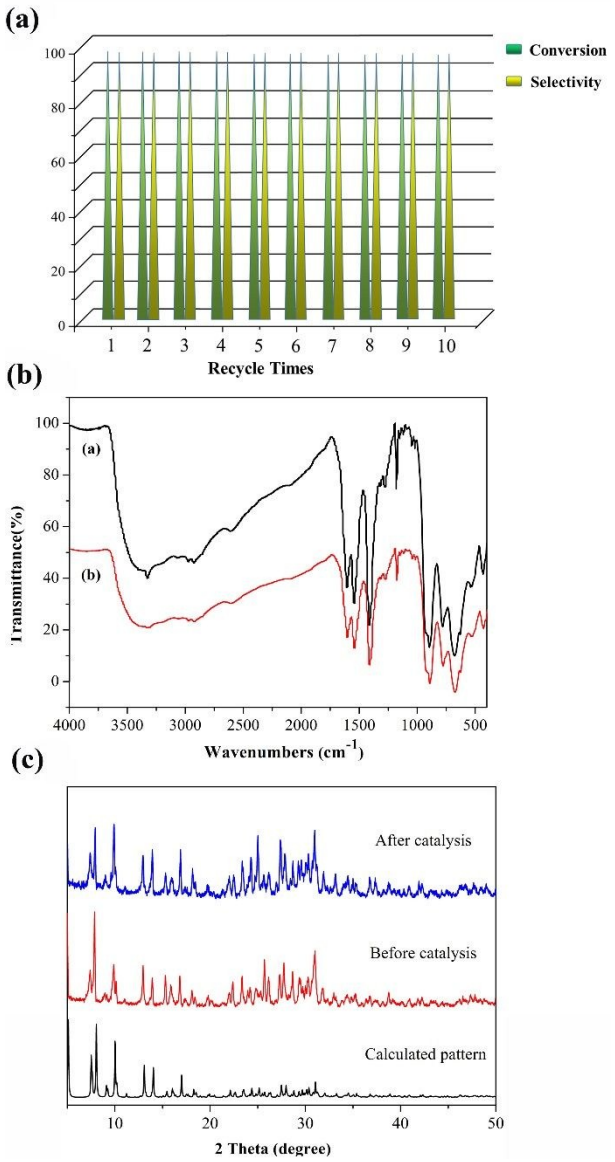


**Fig. 7** a) Recycling of the catalytic system for the oxidation of CEES using compound **1**; b) IR spectrum for (a) as-synthesized compound **1** and (b) recovered catalyst after catalysis reaction; c) Powder X-ray diffraction (PXRD) patterns of **1**: calculated pattern from crystal data (black line); experimental pattern before catalysis (red line); recovered catalyst **1** after 10 catalytic runs of the oxidation of CEES (blue line).

## Catalytic hydrolysis study

As we all know, the broad-spectrum catalyst against CWAs possessing multiple detoxification pathways, such as oxidation and hydrolysis, is highly desired. Then, the hydrolytic degradation of organophosphate-based nerve agent simulant DECP was thus examined since compounds **1**−**12** have metal cations as Lewis acid sites and amino groups have the great effect on the hydrolysis according to the literatures.[7] Fig. 8b, 8c, 8d show the conversion

of the hydrolysis of DECP with compounds **1**−**12**. These

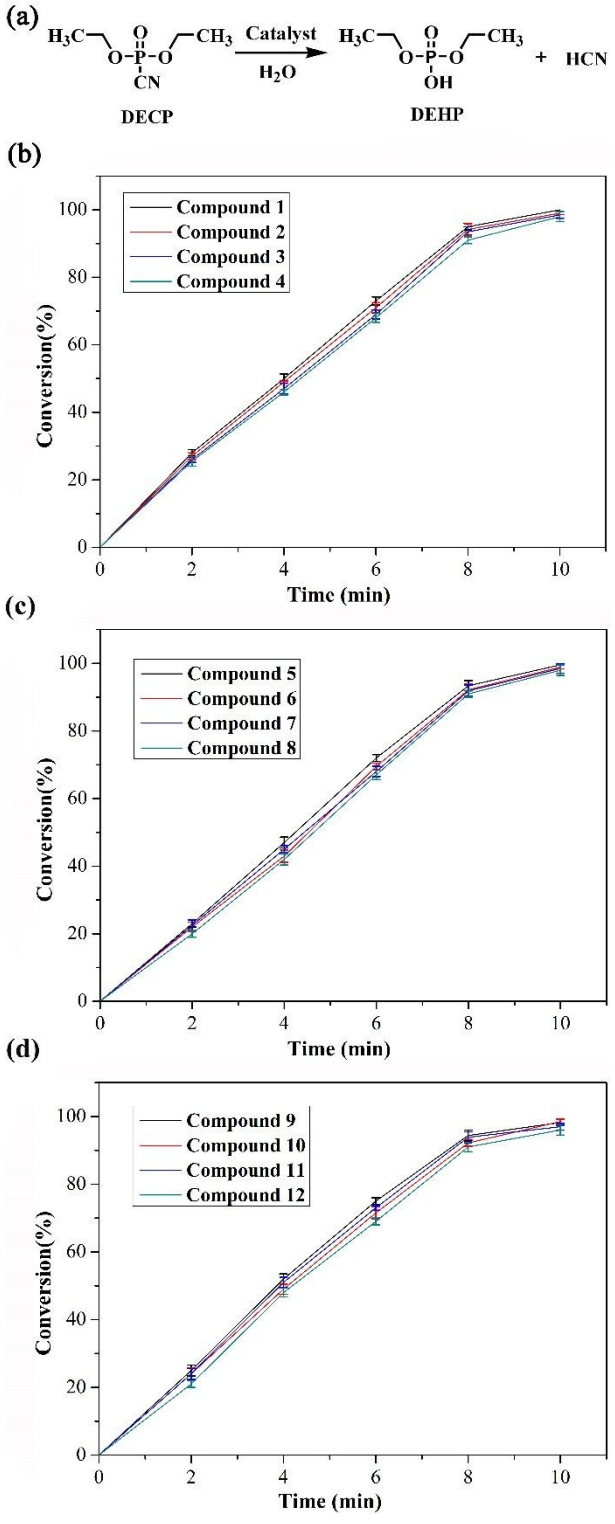


**Fig. 8** a) The hydrolytic decomposition pathway of DECP; b, c, d) The conversion of DECP hydrolysis for compounds **1**−**12**. Reaction conditions: 1 mmol DECP, 0.6 μmol catalyst, 0.25 mmol naphthalene (internal standard), 600 μL DMF and 50 μL $H_2O$ at room temperature for 10 min.

compounds can catalyze the hydrolytic degradation of DECP to the nontoxic diethyl phosphate within 10 minutes under a small amount of catalysts. Compound **1** exhibits the best catalytic activity, and can hydrolyze 100% of DECP into the nontoxic product. The turnover frequency (TOF) of the catalytic degradation reaction using **1** is about 10000 $h^{-1}$ with the half-life of 4.2 min. To our knowledge, this catalytic activity for the degradation of DECP using **1** is significantly higher than most reported catalysts built on POMs. Table 2 displays the comparison of the catalytic hydrolysis activities for DECP among **1**, **5** and **9**. The initial rates were ascertained from the slope of the amount of DECP versus time. The catalytic activities of compounds **1** (100%) and **5** (99.5%) are almost approximate, but the difference of these initial rates (7.8 and 6.9 mM/s) is distinct, which indicates the central hetero atom produces certain effect on the DECP hydrolysis. Under the similar conditions, the catalytic activity of compound **9** (98.2%, 6.3 mM/s) is obviously lower than that of compound **1** (100%, 7.8 mM/s), which might be originated from the carboxylic acid ligands with different structures and reveals that PABA ligand modified POM is more beneficial for the catalytic hydrolysis reaction.

To reveal the active sites of compound **1** for hydrolyzing DECP, the catalytic activities of compound **13** ($K_3[AsMo_6O_{21}(PABA)_3]\cdot nH_2O$) and $CoCl_2$ salt were determined (Fig. S31). Compound **13** can hydrolyze 69.9% of DECP, while $CoCl_2$ converts 51% of DECP to the nontoxic products, which show higher conversion than the blank but much lower activity than compound **1** (100%). The experiment results indicate that both PABA modified POM $\{AsMo_6(PABA)_3\}$ and metal cation as the Lewis acid together enhance the hydrolytic degradation activity. Besides, the catalytic activities of compounds **14** and **15** respectively based on $\{AsMo_6(Ala)_3\}$ and $\{AsMo_6(PHBA)_3\}$ unit for hydrolysing DECP, were detected (Table 2). Compounds **14** and **15** can respectively convert 80.3% and 82.5% of DECP with the initial rates of 4.2 and 4.5 mM/s, which displayed much lower catalytic activity than **1** (100%, 7.8mM/s). The observed difference in the catalytic hydrolysis activity is mainly owing to the covalently bonded carboxylic acid ligands. The PABA ligand with aromatic amine in **1** is more advantageous for the hydrolysis reaction of DECP. Similar phenomenon has also been investigated in metal-organic frameworks by other groups.[7]

**Table 2. Comparison of DECP decomposition by different materials.**

| Catalyst | Conversion (%) | initial rate (mM/s) |
|---|---|---|
| Compound **1** | 100 | 7.8 |
| Compound **5** | 99.5 | 6.9 |
| Compound **9** | 98.2 | 6.3 |
| Compound **13** | 69.9 | 3.6 |
| Compound **14** | 80.3 | 4.2 |
| Compound **15** | 82.5 | 4.5 |

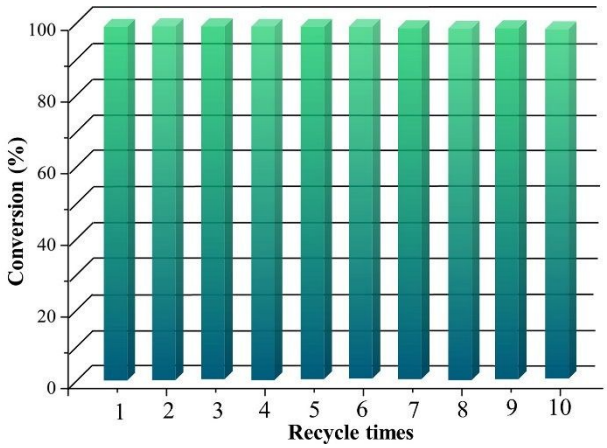


**Fig. 9** Recycling of the catalytic system for the hydrolytic degradation of DECP using compound **1**.

The kinetics of the hydrolytic degradation system using **1** as catalyst was investigated. Fig. S32a, S32c show the conversion of DECP changes under various quantities of substrates and catalysts. And the rates of the catalytic hydrolysis reaction decreased with more substrates or fewer catalysts in Fig. S32 b, d. They also demonstrated the catalytic degradation reaction of DECP conform to the first-order reaction with respect to the substrates and catalysts. The reusability of **1** was studied by circular reaction and proceeding the same operation with the first reaction. The catalytic activity remained stable for the following 10 cycles (Fig. 9). To further investigate the degradation of DECP, $H_2O_2$ was introduced to the catalytic systems for DECP. No obvious change was found in the presence of $H_2O_2$. In addition, the oxidation of CEES and hydrolysis of DECP were performed in the same reaction vessel. The catalytic results show that 96.7% CEES can be converted to the corresponding CEESO with the selectivity of 97.1% and DECP was completely decomposed, indicating both CWA simulants can be simultaneously decomposed to their corresponding products with high efficiency.

## 4. Conclusions

In summary, twelve new hybrid dimers **1**−**12** based on different carboxylic acid ligands modified POMs and metal cations were designedly synthesized, and used as catalysts for rapid destruction of two CWA simulants (CEES and DECP) at room temperature. The excellent catalytic performances of these compounds originate from the synergetic effects among carboxylic acid ligands with pendent amino group, {$AsMo_6$}/ {$TeMo_6$} unit, and transition metal cations. In addition, the comparison study of catalytic activities of these compounds indicates that i) as linker to the polyoxoanion, $Co^{2+}$ cation shows the better catalytic ability than $Zn^{2+}$, $Ni^{2+}$ and $Mn^{2+}$ cation, and the quantity of metal cation will influence the catalytic activities; ii) as organic ligand modified the POM, the PABA ligand with aromatic amine is more advantageous than Ala, Ac and PHBA ligand for the oxidation of CEES and the hydrolysis of DECP; iii) the central heteroatoms (As, Te) of polyoxoanions can also impact their catalytic activities, and with As as heteroatom catalysts have the better activity. This work will help the development of more efficient POM-based materials for destruction of diverse CWAs.

View Article Online
DOI: 10.1039/C9CY00094A

### Conflicts of interest

There are no conflicts to declare.

### Acknowledgements

This work is financially supported by the National Natural Science Foundation of China (21371027, 20901013), Natural Science Foundation of Liaoning Province (2015020232) and Fundamental Research Funds for the Central Universities (DUT15LN18, DUT15LK02).

### References

1 F. M. Raushel, *Nature* 2011, **469**, 310–311.

2 R. D. Gall, C. L. Hill, J. E. Walker, *Chem. Mater.,* 1996, **8,** 2523-2527.

3 Y. C. Yang, J. A. Baker, J. R. Ward, *Chem. Rev*., 1992, **92**, 1729–1743.

4 N. S. Bobbitt, M. L. Mendonca, A. J. Howarth, T. Islamoglu, J. T. Hupp, O. K. Farha, R. Q. Snurr, *Chem. Soc. Rev.,* 2017, **46**, 3357–3385.

5 K. Kibong, G. T. Olga, A. A. David, G. C. David, Chem. Rev., 2011, **111**, 5345-5403.

6 Y. Y. Liu, S. Y. Moom, J. T. Hupp, O. K. Farha, *ACS. Nano*., 2015, **9**, 12358–12364.

7 I. Timur, A. O. Manuel, P. Emmanuel, J. H. Ashlee, A. V. Nicolaas, A. Ahmet, M. A. Abdullah, J. C. Christopher, K. F. Omar, *Angew. Chem. Int. Ed.,* 2018, **57**, 1–6.

8 D. T. Lee, J. J. Zhao, G. W. Peterson, G. N. Parsons, *Chem. Mater*., 2017, **29**, 4894−4903.

9 Y. Q. Li, Q. Gao, Y. S. Zhou, L. L. Zhang, Y. X. Zhong, Y. Ying, M. C. Zhang, Y. Q. Liu, Y. A. Wang. *J. Hazard. Mater.* 2018**,** **358**,113–121.

10 a)D. Waysbort, D. J. McGarvey W. R. Creasy, K. M. Morrissey, D. M. Hendrickson, H. D. Durst. *J. Hazard. Mater.,* 2009, **161** 1114-1121; b) G. W. Wagner, L. R. Procell, D. C. Sorrick, G. E. Lawson, C. M. Wells, C. M. Reynolds, D. B. Ringelberg, K. L. Foley, G. J. Lumetta, D. L. Blanchard, *Ind. Eng. Chem. Res.*, 2010, **49**, 3099–3105; c) M. Verma, R. Chandr, V. K. Gupta. *J. Mol. Liquids.*, 2016, **215**, 285–292; d) F. Carniato, C. Bisio, C. Evangelisti, R. Psaro, V. Dal Santo, D. Costenaro, L. Marchesea and M. Guidotti. *Dalton Trans.,* 2018, **47**, 2939–2948; e) F. Carniato, C. Bisio, R. Psaro, L. Marchese, M. Guidotti. *Angew. Chem. Int. Ed*., 2014, **53**, 10095 –10098.

11 A. Müller, F. Peters, M. T. Pope, D. Gatteschi, *Chem. Rev*., 1998, **98**, 239–272.

12 A. Proust, B. Matt, R. Villanneau, G. Guillemot, P. Gouzerha, G. Izzeta, *Chem. Soc. Rev*., 2012, **41,** 7605–7622.

13 A. M. Khenkin, I. Efremenko, J. M. L. Martin, R. Neumann, *J. Am. Chem. Soc*., 2013, **135,** 19304−19310.

14 K. Kamata, K. Yonehara, Y. Sumida, K. Yamaguchi, S. Hikichi, N. Mizuno, *Science.,* 2003, **300**, 964−966.

15 D. L. Long, E. Burkholder, L. Cronin, *Chem. Soc. Rev.,* 2007, **36,** 105–121.

16 W. J. Luo, J. Hu, H. L. Diao, B. Schwarz, C. Streb, Y. F. Song, *Angew. Chem. Int. Ed.,* 2017, **56**, 4941–4944.

17 Y. J. Tang, M. R. Gao, C. H. Liu, S. L. Li, H. L. Jiang, Y. Q. Lan, M. Han, S. H. Yu, *Angew. Chem. Int. Ed*., 2015, **54**, 12928–12932.

18 H. Yu, S. Ru, G. Y. Dai, Y. Y. Zhai, H. L. Lin, S. Han. Y. G. Wei, *Angew. Chem. Int. Ed*., 2017, **56**, 3867–3871.

19 J. Zhang, J. Hao, Y. G. Wei, F. P. Xiao, P. C. Yin, L. S. Wang, *J. Am. Chem. Soc.*, 2010, **132**, 14−15.

20 S. S. Wang, G. Y. Yang, Recent advances in polyoxomet alate-catalyzed reactions, *Chem. Rev*., 2015, **115**, 4893–4962.

21 a) M. Zhao, X. W. Zhang and C. D. Wu, *ACS Catal.,* 2017, **7**, 6573−6580; b) Y. P. Duan, W. Wei, F. Xiao, Y. Xi, S. L. Chen, J. L. Wang, Y. Q. Xu and C. W. Hu, *Catal. Sci. Technol.,* 2016, **6**, 8540–8547.

22 a) Y. Zhang, L. L. Wu, X. Y. Zhao, Y. N. Zhao, H, Q, Tan, X. Zhao, Y. Y. Ma, Z. Zhao, S. Y. Song, Y. H, Wang, Y, G, Li, *Adv. Mater.* 2018 1801139; b) X. L. Hao, Y. Y. Ma, H. Y. Zang, Y. H. Wang, Y. G. Li, and, E. B. Wang, *Chem. Eur. J.,* 2015, **21**, 3778 – 3784

23 M. Zheng, Y. Ding, X. H. Cao, T. Tian, J. Q. Lin, *Appl. Catal. B: Environ.,* 2018, **237**, 1091–1100.

24 a) Y. Wang, B. Li, H. J. Qian, L. X. Wu, *Inorg. Chem*., 2016, **55**, 4271−4277; b) P. C. Yin, A. Bayaguud, P. Cheng, F. Haso, L. Hu, J. Wang, D. Vezenov, R. E. Winans, J. Hao, T. Li, Y. G. Wei, and T. B. Liu, *Chem. Eur. J.,* 2014, **20**, 9589 – 9595

25 a) P. T. Ma, F. Hu, J. P. Wang, J. Y. Niu, *Coord. Chem. Rev*., 2019, **378**, 281-309; b) M. D. Han, Y. J. Niu, R. Wan, Q. F. Xu, J. K. Lu, P. T. Ma, C. Zhang, J. Y. Niu, and J. P.Wang, *Chem. Eur. J*., 2018, **24***,* 11059–11066; c) J. W. Wang, Y. J. Niu, M. Zhang, P. T. Ma, C. Zhang, J. Y. Niu, and J. P. Wang. *Inorg. Chem*., 2018, **57**, 1796−1805.

26 X. B. Han, Y. G. Li, Z. M. Zhang, H. Q. Tan, Y. Lu, E. B. Wang, *J. Am. Chem. Soc*., 2015, **137**, 5486−5493.

27 R. D. Gall, M. Faraj, and C. L. Hill, *Inorg. Chem*., 1994, **33**, 5015-5021.

28 W. W. Guo, H. J. Lv, K. P. Sullivan, W. O. Gordon, A. Balboa, G. W. Wagner, D. G. Musaev, J. Bacsa, C. L. Hill, *Angew. Chem. Int. Ed.,* 2016, **55**, 7403–7407.

29 Da. L. Collins-Wildman, M. Kim, K. P. Sullivan, A. M. Plonka, A. I. Frenkel, D. G. Musaev, and C. L. Hill, *ACS Catal*., 2018, **8**, 7068−7076.

30 M. K. Kinnan, W. R. Creasy, L. B. Fullmer, H. L. Schreuder Gibson, M. Nyman, *Eur. J. Inorg. Chem*., 2014, 2361–2367.

31 a) J. Dong, J. F. Hu, Y. N. Chi, Z. G. Lin, B. Zou, S. Yang, C. L. Hill, C. W. Hu, *Angew. Chem. Int. Ed*., 2017, **56**, 4473–4477; b) J. Dong, H. J. Lv, X. R. Sun, Y. Wang, Y. M. Ni, B. Zou, N. Zhang, A.X. Yin, Y. N. Chi, C. W. Hu. *Chem. Eur. J.* 2018, **24**, 19208–19215.

32 X. Q. Lia, J. Liu, H. F. Dong, X. R. Sun, Y. N. Chi, C. W. Hu, *J. Hazard. Mater.,* 2018, **344**, 994–999.

33 F. J. Ma, S. X. Liu, C. Y. Sun, D. D. Liang, G. J. Ren, F. Wei, Y. G. Chen, Z. M. Su, *J. Am. Chem. Soc*., 2011, **133**, 4178–4181.

34 C. T. Buru, P. Li, B. L. Mehdi, A. Dohnalkova, A. E. Platero-Prats, N. D. Browning, K. W. Chapman, J. T. Hupp, O. K. Farha, *Chem. Mater*., 2017, **29**, 5174–5181.

35 Y. Q. Li, Q. Gao, L. J. Zhang, Y. S. Zhou, Y. X. Zhong, Y. Ying, M. C. Zhang, C. Q Huang and Y. A. Wang, *Dalton Trans.*, 2018., **47**, 6394–6403.

36 K. P. Sullivan, W. A. Neiwert, H. D. Zeng, A. K. Mehta, Q. S. Yin, D. A. Hillesheim, S. Vivek, P. C. Yin, D. L. Collins-Wildman, E. R. Weeks, T. B. Liu and C. L. Hill, *Chem. Commun.,* 2017, **53**, 11480-11483.

37 Y. J. Hou, H. Y. An, Y. M. Zhang, T. Hu, W. Yang, and S. Z. Chang, *ACS Catal.,* 2018, **8**, 6062−6069.

38 a) C. A. Ohlin, E. M. Villa, J. C. Fettinger, W. H. Casey, *Angew. Chem. Int. Ed.,* 2008, **47**, 8251–8254; b) N. Mizuno, K. Kamata, Coord. *Chem. Rev.,* 2011, **255**, 2358–2370.

39 Y. Y. Liu, C. T. Buru, A. J. Howarth, J. J. Mahle, J. H. Buchanan, J. B. DeCoste, J. T. Hupp, O. K. Farha. J. Mater. Chem. A, 2016, **4**, 13809–13813

View Article Online
DOI: 10.1039/C9CY00094A

# Versatile catalysts constructed from hybrid polyoxomolybdates for simultaneously detoxifying sulfur mustard and organophosphate simulants

Yujiao Hou, Haiyan An,* Shenzhen Chang, Jie Zhang

College of Chemistry Dalian University of Technology, Dalian 116023, P. R. China

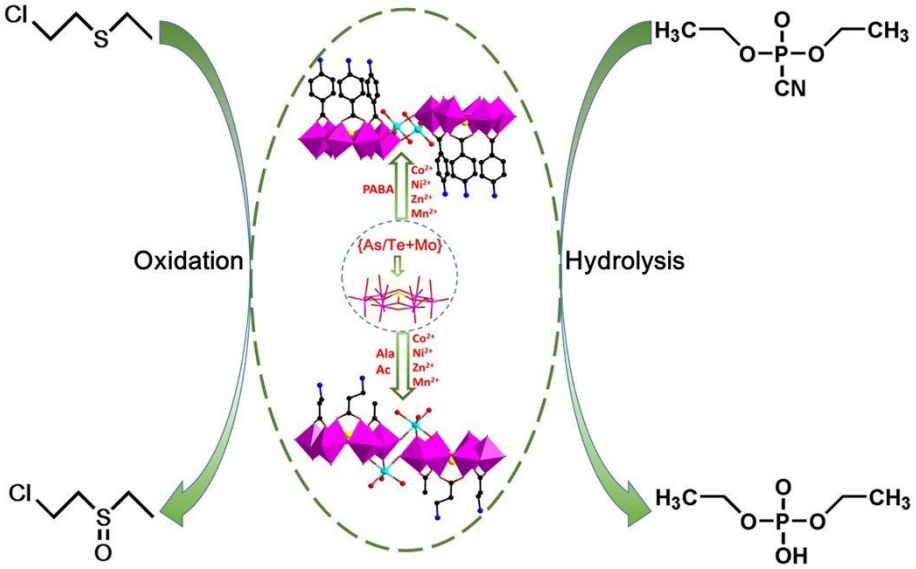


Twelve new hybrid dimers based on carboxylic acid ligands modified polyoxomolybdates were prepared, which can rapidly oxidize the mustard gas simulant, CEES, and hydrolyze the nerve agent simulant, DECP, at room temperature.